Transactions on the Built Environment vol 22, © 1996 WIT Press, www.witpress.com, ISSN 1743-3509

CTH hydrocode predictions on the effect of rod nose-shape on the velocity at which tungsten alloy rods transition from rigid body to eroding penetrators when impacting thick aluminium targets

D.R. Scheffler
U.S. Army Research Laboratory, ATTN:AMSRL-WT-TC, Aberdeen Proving Ground, MD 21005-5066, USA

Abstract

This study examines the ability of the CTH hydrocode to predict the effect of rod nose-shape on the transition from rigid body to eroding rod penetration for tungsten alloy long rods penetrating or perforating thick aluminum targets. Two rod nose-shapes and two target alloys were considered. The rod nose-shapes were hemispherical and ogival, and the target alloys were 53.34 cm thick 5083 aluminum and 7039 aluminum. Results are compared to an experimental study that delineated the effect of nose-shape on the threshold velocity at which tungsten alloy penetrators transition from rigid body to eroding rod when penetrating thick aluminum targets. Predictions of the threshold velocity for the ogival-nose rods are offered in advance of the ballistic experiments.

1 Introduction

Zukas[1], in examining the convergence characteristics of the Eulerian CTH hydrocode[2] as a function of spacial resolution, found that the code could not accurately predict perforation of armor plate by a hard projectile at low velocities (less then 1.5 km/s). Previously, this problem had been modeled successfully using an in-house version of the EPIC Lagrangian hydrocode. Zukas observed that, regardless of the mixed cell strength formulation used (several are available in the CTH hydrocode), high-strength penetrator material included in a mixed cell was treated unrealistically as being significantly softer and thereby leading to deformation of the penetrator. The net effect was that the CTH hydrocode could not accurately model the rigid body penetration of a soft target, the eroding penetration of harder targets at low velocities, or the sliding between two material interfaces.

A new boundary layer algorithm for sliding interfaces (BLINT) was recently incorporated into the CTH hydrocode for two-dimensional problems only[3]. The algorithm relocates the slip layer outside of the mixed cells and into the softer material, thus allowing hard materials to penetrate as rigid bodies. Good results have been obtained using the BLINT algorithm by Silling[4] and Kmetyk and Yarrington[5]. Both modeled hard penetrators impacting soft targets knowing *a priori* that the penetrators would remain rigid.

This study examines the ability of the CTH hydrocode (August 1993 release) to predict the impact velocity at which the penetrator will transition from rigid body to eroding rod and the effect of the penetrators nose-shape on this transition velocity. The perforation of soft aluminum targets by tungsten alloy (95W-2.5Ni-1.0Fe-1.5Co, cold worked by swaging to a 21% reduction-in-area) long rods was modeled. To gauge the accuracy of the CTH hydrocode with the BLINT algorithm, the simulation results are compared to the experimental depth of penetration tests[6]. Two rod nose-shapes and two target alloys were considered. The rod nose-shapes were hemispherical and ogival, and the target alloys were 53.34 cm thick 5083 aluminum and 7039 aluminum.

The CTH hydrocode is a state-of-the-art, second-order accurate, Eulerian hydrocode developed by Sandia National Laboratories that is capable of solving complex problems in shock physics in one, two, or three dimensions. The code provides several constitutive models, including an elastic-perfectly-plastic model with provisions for work hardening and thermal softening, the Johnson-Cook model[7], the Zerilli-Armstrong model[8], the Steinberg-Guinan-Lund model[9,10], and an undocumented power-law model. High explosive detonation can be modeled using the programmed burn model, the Chapman-Jouguet volume burn models, or the history variable reactive burn model[11]. Several equation of state (EOS) options are available, including tabular (i.e., SESAME), analytical (ANEOS), Mie-Gruneisen, and Jones-Wilkins-Lee (JWL)[12]. Material failure occurs when a threshold value of tensile stress or hydrostatic pressure is exceeded. In addition, the Johnson-Cook failure model[13] is also available. When failure occurs in a cell, void is introduced until the stress state of the cell is reduced to zero. Recompression is permitted. To reduce the diffusion typically encountered in Eulerian simulations, several advanced material interface tracking algorithms are provided, including the high resolution interface tracking (HRIT) algorithm (available for two-dimensional simulations only), the simple line interface calculation (SLIC) algorithm[14], and the Sandia modified Youngs' reconstruction algorithm[15] (SMYRA).

2 Problem setup

The geometries for the tungsten alloy penetrators are shown in Figure 1. The ogival-nose penetrator has a length of 10.1346 cm and a diameter of 0.67568 cm. The length of the hemi-nose penetrator was shortened to 9.779 cm such

Transactions on the Built Environment vol 22, © 1996 WIT Press, www.witpress.com, ISSN 1743-3509

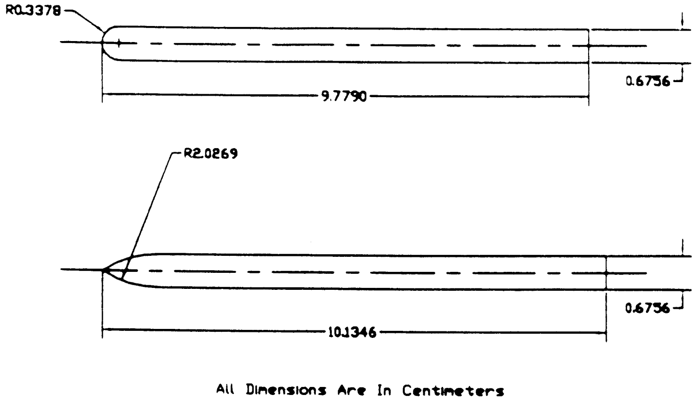

Figure 1. Penetrator geometries.

that both penetrators had the same nominal mass of 63 g.

Three different constitutive models were used in the simulations to model the deviatoric response of the materials. The choice of the constitutive model used for a material was governed by the availability of material data. Material data was not available for the 95W-2.5Ni-1.0Fe-1.5Co, 21% swaged tungsten alloy penetrators used in the experiments; therefore, the alloy was approximated using 95W-3.5Ni-1.5Fe tungsten alloy data for the Steinberg-Guinan-Lund strain rate independent model reported in Steinberg[16]. This tungsten alloy has the same percentage of tungsten and the same approximate density as the 95W-3.5Ni-1.0Fe-1.5Co, 21% swaged alloy. For the 7039 aluminum target, the Johnson-Cook constitutive model was used with parameters reported in Johnson and Cook[7]. For the 5083 aluminum target, a power-law constitutive model was used with parameters reported in Silling[3] and originally reported in Forrestal, Luk, and Brar[17].

The Mie-Gruneisen EOS was used for all materials. EOS data was obtained from a data file provided with the CTH hydrocode. The EOS parameters for 5083 aluminum, 7039 aluminum, and 95% tungsten content tungsten alloy were not available; therefore, they were approximated using parameters for 6061 aluminum, 7075 aluminum, and 90W-7Ni-3Fe tungsten alloy, respectively. The initial density of the 6061 and the 7075 aluminum alloys were changed to reflect those for 5083 and 7039 aluminum as reported in the Metals Handbook Desk Edition[18]. The initial density of the 90W-7Ni-3Fe alloy was changed to reflect the initial density of the 95W-3.5Ni-1.5Fe alloy reported in Steinberg[16]. For the reader's convenience, the EOS parameters used for all materials are listed in Table 1.

Failure in most the simulations was modeled using a threshold tensile pressure criteria. The tensile pressure at which the tungsten alloy, the 5083 aluminum, and the 7039 aluminum were assumed to fail was 3.5 GPa,

Table 1. Equation of state parameters.

Material	Density ρ_o (g/cm^3)	Sound Speed c_o (km/s)	U_s-U_p Slope	Gruneisen Parameter Γ_o	Specific Heat c_v (erg/g/eV)
W Alloy	18.16	4.03	1.237	1.67	1.66e11
5083 Al	2.66	5.34	1.40	1.97	1.07e11
7039 Al	2.77	5.20	1.36	2.20	1.07e11

0.45 GPa, and 0.50 GPa, respectively.

All simulations used a two-dimensional cylindrical coordinate mesh consisting of 85 x 1545 cells. The radial direction mesh starts at the axis of symmetry of the penetrator with a constant cell size of 0.0422275 cm out to a radius of 1.6891 cm. Thereafter, the dimensions of the cells expand by 5% increments out to the outer radius of the target. This mesh provides eight cells across the radius of the penetrator. The axial direction mesh has a constant cell size of 0.0422275 cm; thus, cells in the penetrator-target interaction region have a one-to-one aspect ratio.

Parameters for the BLINT model were chosen to be similar to those reported in Kmetyk and Yarrington[5]. Thus the boundary layer thickness, w_{bl}, and the slip layer thickness, w_{sl}, were chosen to be twice the zone size of cells in the penetrator-target interaction region. An option to automatically increase the yield strength of the penetrator material by a factor equal to

$$\left(\frac{\rho_o + w_{bl}}{\rho_o}\right)^2$$

(where ρ_0 is the initial density of the hard material) was used. This option was used because numerical noise can cause shear stresses close to the yield stress to exceed the yield stress, causing premature irreversible deformation of the penetrator. An additional option allows for the inclusion of friction; however, friction between the target and penetrator were not modeled in this study. Kmetyk and Yarrington[5] showed that the BLINT model tended to overpredict penetration in deep penetration problems unless friction was included.

The CTH hydrocode cannot convect velocity in a manner such that both momentum and kinetic energy are both conserved exactly. The default option allows conservation of kinetic energy such that total energy is conserved during the convection phase of a computational cycle; however, momentum is not conserved. A second option convects velocity such that momentum is conserved during the convection phase of a computational cycle and any kinetic energy discrepancies are discarded. Simulations were run for both of

Transactions on the Built Environment vol 22, © 1996 WIT Press, www.witpress.com, ISSN 1743-3509

Table 2. Initial impact conditions and ballistic test results.

Shot No.	Total Yaw (°)	Striking Velocity (m/s)	Original Mass (g)	Penetration (cm)
Hemi-Nose Penetrator vs. 7039 Aluminum Target				
4338	0.50	1,165	62.7	11.4est.
4339	0.25	1,038	63.1	28.3
4340	0.50	1,248	63.1	13.0
Ogival-Nose Penetrator vs. 7039 Aluminum Target				
4341	0.90	1,156	63.4	37.7
4342	0.56	1,291	63.4	>53.3
4343	0.71	1,075	63.1	35.4
Hemi-Nose Penetrator vs. 5083 Aluminum Target				
4344	0.50	1,086	62.8	44.8
4345	0.35	1,200	63.0	20.0
4346	0.25	1,296	62.9	21.6
Ogival-Nose Penetrator vs. 5083 Aluminum Target				
4347	0.50	923	62.9	41.7
4348	1.12	1,070	63.1	39.9
4349	0.80	1,227	62.8	>53.3

these convection options. Simulations that conserved kinetic energy during the convection phase of a computational cycle will be referred to as KE Sim(s), and those conserving momentum during the convection phase of a computational cycle will be referred to as MV Sim(s). A final option conserves both momentum and total energy during the convection phase of a computational cycle by depositing the kinetic energy discrepancy into internal energy. This can have the effect of artificially heating a material, and therefore, this option was not used.

3 Results and discussion

Initial impact conditions and ballistic test results[6] from the experiments are provided in Table 2. The penetration depths listed were measured perpendicular to the original target surface along the penetrator's original flight line. In some cases, the penetrators wandered within the thick aluminum targets, therefore, the total path length taken by the penetrators may have been greater than the listed penetration depth. The total yaws for the penetrators were quite small (in most cases less than 1°). However, these yaw values still exceed the critical yaw as defined in Bjerke et al.[19,20] since the penetration channel diameter is about the same as the penetrator shank diameter for rigid body penetration of soft targets (e.g., see Forrestal et al.[21]). Any effects of yaw were not treated in these two-dimensional simulations.

For rigid body long-rod penetrators penetrating soft targets, the increase in penetration depth is nearly directly proportional to the striking velocity, except at extremely low striking velocities (less then 600 m/s). However, as impact velocities are further increased, the stresses on the penetrator will eventually exceed the yield strength of the penetrator material. The penetrator will begin to deform plastically, and the increase in penetration with increasing striking velocity ceases to be nearly linear. The deformation and erosion of the penetrator at these higher velocities leads to a dramatic drop in the penetration depth. Still further increases in striking velocity will again result in a second region displaying a near linear increase in penetration depth with increasing striking velocity. The plot of penetration depth as a function of impact velocity will eventually level off as the penetrator approaches the hydrodynamic limit given by

$$L_0\left(\frac{\rho_p}{\rho_t}\right)^{\frac{1}{2}}$$

where L_0 is the initial rod length and ρ_p and ρ_t are the penetrator and target densities, respectively.

Experimental results as well as the predictions from the KE Sims and the MV Sims for the 5083 and 7039 aluminum targets are shown in Figures 2a and 2b, respectively. The experimental results are represented with solid symbols, the KE Sims are represented with hollow symbols, and the MV Sims are represented with half-filled symbols. In addition, the hemi-nose penetrators are represented by circles, the ogival-nose penetrators are represented by squares, and the rear of the target is represented with a dotted line. If a penetrator perforated the target, it is represented by an error bar on the symbol. Examining only the predictions of the hemi-nose penetrators in Figures 2a and 2b, it is apparent that both the KE Sims and the MV Sims seem to predict the same trends seen experimentally. The KE Sims more accurately predicted the transition velocity from rigid body to eroding rod penetration (reflected in the drops in penetration depths). The MV Sims predicted the transition would occur at approximately a 100 m/s higher impact velocity and appear to consistently overpredict the final depths of penetration

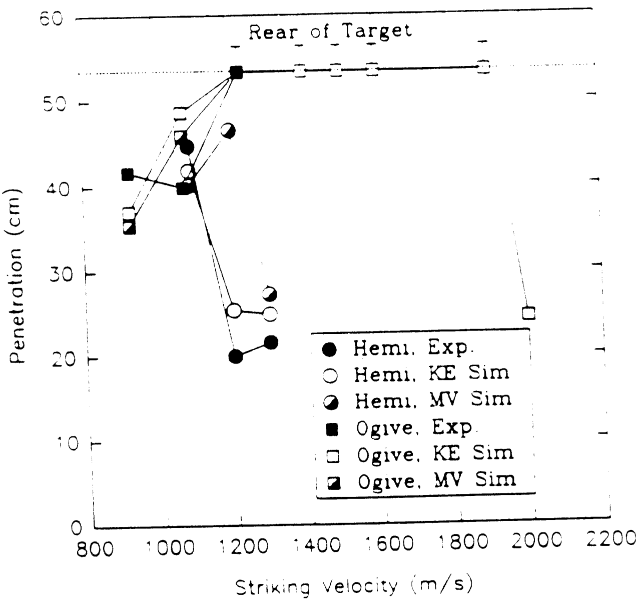

(a)

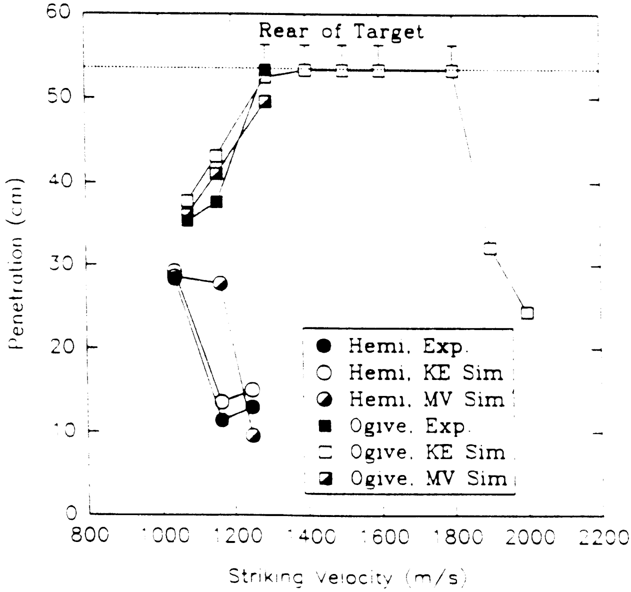

(b)

Figure 2. Comparison of KE Sims and MV Sims with experiment: (a) 5083 aluminum targets; (b) 7039 aluminum targets.

at most velocities. This may be due, in part, to the KE Sims more accurately predicting the projectile shape than the MV Sims (e.g. see Scheffler[22]). For this reason, it was decided to predict the threshold velocity at which the ogival-nose penetrators transition from rigid rod to eroding penetrator using only the KE Sims. The CTH hydrocode runs predicted that the transition velocities would lie between 1,900 and 2,000 m/s for the 5083 aluminum targets and between 1,800 and 1,900 m/s for the 7039 aluminum targets. Future ballistic experiments will attempt to confirm these predictions. Limited testing against thinner targets[6] has confirmed that the transition velocities lie above 1,700 m/s for both aluminum alloys.

While the CTH hydrocode seems to have done an adequate job of predicting the threshold velocity at which hemi-nose penetrators transition from rigid body to eroding rods, it tended to overpredict the actual penetration values. This may have been due, in part, to the exclusion of friction in the simulations. The BLINT model was added to the CTH hydrocode in order to model rigid body penetration; therefore, once the transition to eroding rod penetration occurs the model may no longer be necessary or accurate. For this reason, the KE Sims for which the BLINT model seemed to predict erosion were redone with the BLINT model turned off. Results of these simulations are shown in Figures 3a and 3b for the 5083 and 7039 aluminum targets, respectively. The symbols in Figure 3 are the same as those in Figure 2 with the exception that half-filled symbols represent simulations where the BLINT model was turned off. In examining the figures, it is apparent that all of the simulations with the BLINT turned off underpredict experiment. This may, in part, be due to the fact that the option in the BLINT model to increase the penetrator's yield strength was no longer in use and, in part, due to the mixed cell treatment artificially reducing the strength of penetrator material in mixed cells. The difference between prediction and experiment is less for the ogival-nose rods because the influence of material strength is less at higher impact velocities.

While the results so far seem to suggest that the BLINT model seems to predict, at least for the hemi-nose KE Sims, when the transition from rigid body to eroding rod occurs, it does not show the penetrators eroding in their typical mushroom head fashion. Instead, the penetrators simply deformed with little, if any, noticeble erosion occuring. Magness[23] suggested that the threshold tensile pressure failure model used might be the cause. Reasons for this are given in the significant paper by Magness[24] discussing the properties of kinetic energy penetrators. To investigate the effect of the failure model, all simulations for the hemi-nose penetrator impacting 5083 aluminum at a striking velocity of 1,296 m/s were redone using the Johnson-Cook failure model with all but the first parameter turned off. All material would now be set to fail at a strain of 150%. Final projectile shapes are shown in Figure 4. Only the projectile material is shown in Figure 4 in order to easily see the erosion products. The projectiles are designated XX-XX-X, where the first two X's represent KE Sim (KE) or MV Sim (MV), the second set of X's represent

Transactions on the Built Environment vol 22, © 1996 WIT Press, www.witpress.com, ISSN 1743-3509

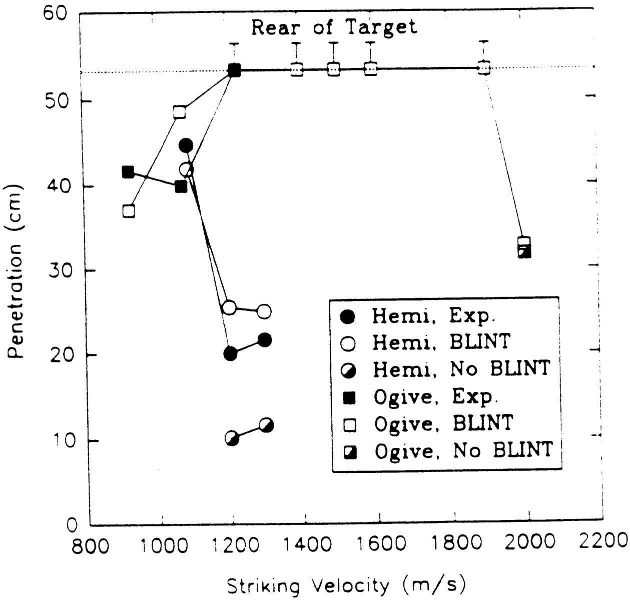

(a)

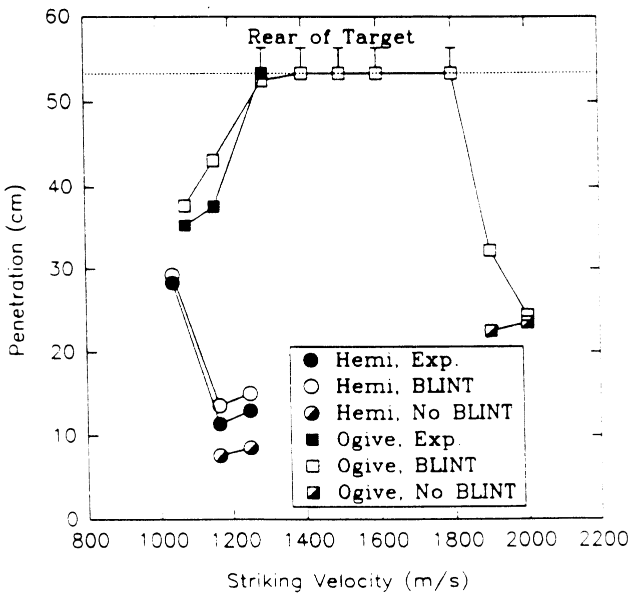

(b)

Figure 3. Comparison of KE Sims with and without BLINT model with experiment: (a) 5083 aluminum targets; (b) 7039 aluminum targets.

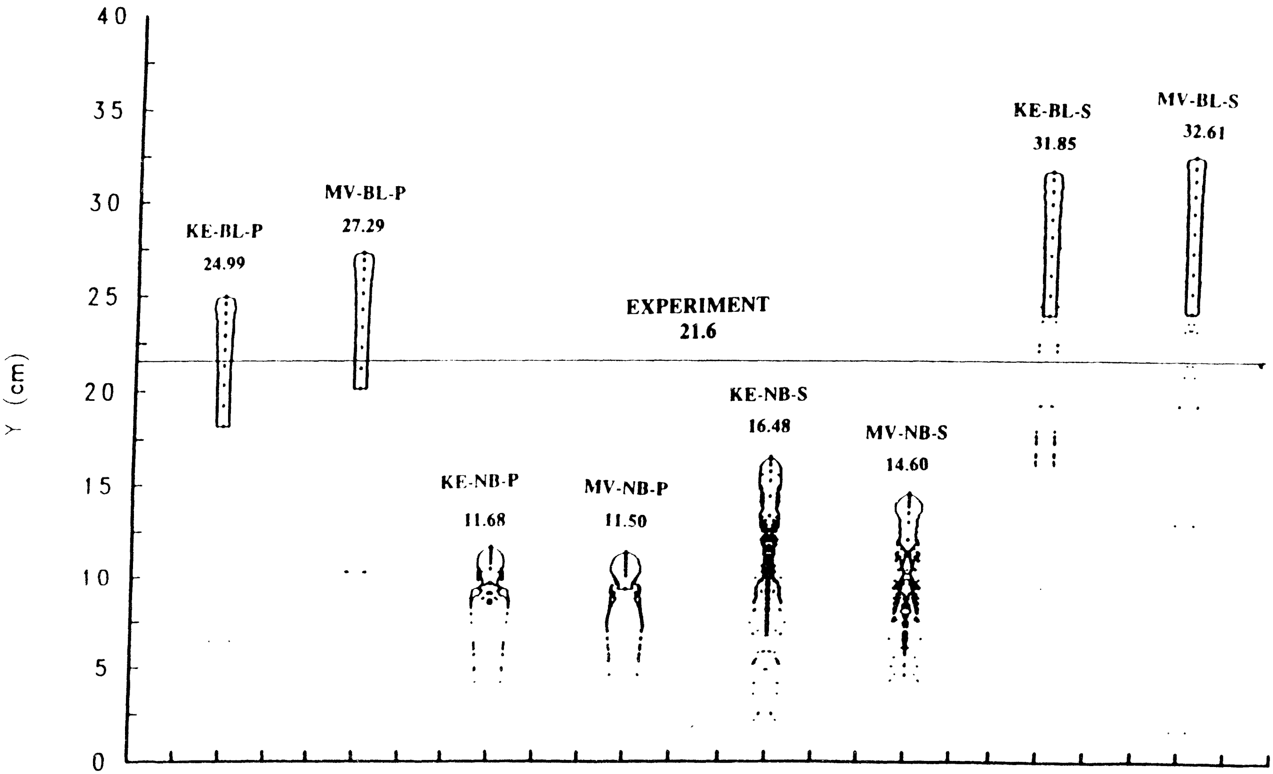

Figure 4. Comparison of all simulations of the hemi-nose penetrator against a 5083 aluminum target with an impact velocity of 1,296 m/s.

BLINT model (BL) or no BLINT model (NB), and the final X represents threshold tensile pressure failure model (P) or threshold strain model using Johnson-Cook failure (S). Thus, a designation of KE-BL-P means the simulation was a KE Sim, with the BLINT model turn on, and using the threshold tensile pressure failure model. Under the projectile designation is the predicted penetration depth in centimeters. Experimentally, the penetration was 21.6 cm and is represented with a horizontal line in Figure 4. The y-axis in Figure 4 represents the penetration depth.

From Figure 4, it is apparent that very little erosion took place in the KE-BL-P and MV-BL-P simulations (KE Sim and MV Sim from Figure 2) and that the drastic drop in penetration seen in Figure 2 was due to plastic deformation. Turning the BLINT model off caused a more typical erosion event to occur, but also caused excessive deformation in the penetrator (KE-NB-P and MV-NB-P simulations). Keeping the BLINT model turned off and changing to a strain-based failure model increased the predicted penetration values, and the deformation of the penetrator more closely resembled those seen in Magness[24]. With the BLINT model turned on and using a strain-based failure model, the simulations show that some erosion occurred but not as much as expected and the final depths of penetration were overpredicted (KE-BL-S and MV-BL-S simulations). In all cases, the KE Sims' predictions were closer to the experimental result than were their MV Sims counterparts.

4 Conclusions

It is known that the constitutive response of tungsten alloy is dependent on strain, strain rate, percentage tungsten content, tungsten grain size, and amount of swaging[25]. In addition, for solid-solid impacts at velocities of 500 to 2,000 m/s, initial impact pressures rapidly decay to values comparable to the strength of the material; therefore, the constitutive model is of primary importance and the EOS is of secondary importance[26]. It is therefore probably unrealistic to expect the results of simulations, with the constitutive model approximations and simple failure models used for the 95W-2.5Ni-1.0Fe-1.5Co, 21% swaged alloy, to provide an exact match with the experimental data. Nevertheless, the following conclusions are offered.

The BLINT model represents an improvement in the predictive capabilities of the CTH hydrocode for certain types of penetration scenarios, such as rigid body penetrations. The code seems to be able to predict the effect on rod nose shape on the threshold velocity at which transition from rigid body to eroding rod penetration occurs. The predicted transition velocity was determined from seeing a dramatic drop in penetration depth occurring with increasing impact velocity. Predictions for the transition from rigid body to eroding body penetration are offered in advance of the experiments for the ogival-nose penetrators. The simulations predict the transition occurs at impact velocities between 1,900 and 2,000 m/s for the 5083 aluminum targets and at impact velocities between 1,800 and 1,900 m/s for the 7039 aluminum targets. Completion of the experimental test should confirm or refute the predicted values.

In general, the KE Sims did much better than the MV Sims at predicting the velocity at which hemi-nose penetrators transition from rigid body to eroding rod and at predicting the final penetration depths. KE Sims did better than their MV Sims counterparts in predicting the final penetration depths in the study comparing failure models and in the study comparing simulations with and without the BLINT model.

5 Acknowledgments

The author would like to thank Mr. Kent D. Kimsey and Mr. Todd W. Bjerke for their helpful comments and suggestions regarding this paper. The author would especially like to thank Dr. Lee S. Magness Jr. for his helpful advice regarding the direction of research taken, his willingness to discuss and share his work, and assuring the accuracy of my discussion of his experiments. Additional thanks go to Dr. Stewart A. Silling of Sandia National Laboratories for discussions regarding his boundary layer interface algorithm and for providing me with an advanced copy of parts of his user manual.

6 References

1. Zukas, J. A. U.S. Army Research Laboratory Memorandum, Aberdeen Proving Ground, Maryland, U.S.A., 1991.
2. Mc Glaun, J. M., Thompson, S. L., & Elrick, M. G. CTH: a three-dimensional shock wave physics code, *International Journal of Impact Engineering*, 1990, **10** (1-4), 251-360.
3. Silling, S. A. CTH reference manual: boundary layer algorithm for sliding in two dimensions, *SAND93-2487*, Sandia National Laboratories, Albuquerque, New Mexico, U.S.A., 1994.
4. Silling, S. A. Eulerian simulation of the perforation of aluminum plates by nondeforming projectiles, *SAND92-0493*, Sandia National Laboratories, Albuquerque, New Mexico, U.S.A., 1992.
5. Kmetyk, L. N. & Yarrington, P. CTH analyses of steel rod penetration into aluminum and concrete targets with comparisons to experimental data, *SAND94-1498*, Sandia National Laboratories, Albuquerque, New Mexico, U.S.A., 1994.
6. Magness Jr., L. S. Unpublished work.
7. Johnson, G. R. & Cook, W. H. A constitutive model and data subjected to large strains, high strain rates and high temperatures, *Proceedings of the Seventh International Symposium on Ballistics*, The Hague, The Netherlands, 1983.
8. Zerilli, F. J. & Armstrong, R. W. Dislocation-mechanics-based

constitutive relations for material dynamics calculations, *Journal of Applied Physics*, 1987, **61** (5), 1816-1825.
9. Steinberg, D. J. & Lund, C. M. A constitutive model for strain rates from 10^{-4} to 10^{6} s^{-1}, *Journal of Applied Physics*, 1989, **65** (4), 1528-1533.
10. Steinberg, D. J., Cochran, S. G. & Guinan, M. W. A constitutive model for metal applicable at high-strain rate, *Journal of Applied Physics*, 1980, **51** (3), 1498-1504.
11. Kerley, G. I. CTH equation of state package: porosity and reactive burn models, *SAND92-0553*, Sandia National Laboratories, Albuquerque, New Mexico, U.S.A., 1992.
12. Lee, E. L., Hornig, H. C. & Kury, J. W. Adiabatic expansion of high explosive detonation products, *UCRL-50422*, Lawrence Livermore National Laboratory, Livermore, California, U.S.A., 1968.
13. Johnson, G. R. & Cook, W. H. Fracture characteristics of three metals subjected to various strains, strain rates, temperatures, and pressures, *Journal of Engineering Fracture Mechanics*, 1985, **21** (1), 31-48.
14. Noh, W. F. & Woodward, P. SLIC (simple line interface calculation), *Lecture Notes in Physics*, Vol. 59, Springer-Verlag, Berlin, 1976.
15. Bell, R. L. & Hertel Jr., E. S. An improved material interface reconstruction algorithm for eulerian codes, *SAND92-1716*, Sandia National Laboratories, Albuquerque, New Mexico, U.S.A., 1992.
16. Steinberg, D. J., Equation of state and strength properties of selected materials, *UCRL-MA-106439*, Lawrence Livermore National Laboratory, Livermore, California, U.S.A., 1991.
17. Forrestal, M. J., Luk, V. K. & Brar, N. S. Perforation of aluminum armor plates with conical-nose projectiles, *Mechanics of Materials*, 1990, **10** (1-2), 97-105.
18. Boyer, H. E. & Gall T. L. (Eds) *Metals Handbook Desk Edition*, American Society for Metals, Metals Park, Ohio, 1985.
19. Bjerke, T. W., Silsby, G. F., Scheffler, D. R. & Mudd, R. M. Yawed long rod armor penetration at ordnance and higher velocities, *BRL-TR-3221*, U.S. Army Ballistic Research Laboratory, Aberdeen Proving Ground, Maryland, U.S.A., 1991.
20. Bjerke, T. W., Silsby, G. F., Scheffler, D. R. & Mudd, R. M. Yawed long- rod armor penetration, *International Journal of Impact Engineering*, 1992, **12** (2), 281-292.
21. Forrestal, M. J., Tzou, D. Y., Askari, E. & Longscope, D. B. Penetration into ductile matel targets with rigid spherical-nose rods, *International Journal of Impact Engineering*, 1995, **16** (5-6), 699-710.
22. Scheffler, D. R. CTH hydrocode simulations of hemisperical and ogival nose tungsten alloy penetrators perforating finite aluminum targets, in 1996 ASME Pressure Vessel and Piping Conference, *Proceedings of the Structures Under Extreme Loading Conditions*, Montreal, Quebec, Canada, July 21-26, 1996, excepted for presentation.
23. Magness Jr., L. S. Private communication.

Transactions on the Built Environment vol 22, © 1996 WIT Press, www.witpress.com, ISSN 1743-3509

24. Magness Jr., L. S. Properties and performance of ke penetrator materials, in Tungsten & Tungsten Alloys-1992 (ed A. Bose & R. J. Dowding), pp 15-22, *Proceedings of the First International Conference on Tungsten and Tungsten Alloys*, Arlington, Virginia, U.S.A., 1992, Metal Powder Industries Federation, Princeton, New Jersey, U.S.A., 1993.
25. Coates, R. S. & Ramesh, K. T. The deformation of tungsten alloys at high strain rates, in Shock-Wave and High-Strain-Rate Phenomena in Metarials (ed M. A. Meyers, L. E. Murr & K. P. Staudhammer), pp. 203-212, *Proceedings of the International Conference on the Material Effects of Shock-Wave and High-Strain-Rate Phenomena*, San Diego, California, U.S.A., 1990, Marcel Dekker, Inc., New York, New York, 1992.
26. Zukas, J. A., Nicholas, T., Swift, L. B. & Curran, D. R. Impact Dynamics, Wiley-Interscience, New York, 1982.